TECHNISCHE MECHANIK, Band 23, Heft 2-4, (2003), 195-204
Manuskripteingang: 05. Juni 2003

# Contact Strength and Fracture Toughness from Opposite Cylinder Loading Tests

T. Fett, D. Munz

*Bars loaded by oppositely concentrated forces via rollers are appropriate test specimens for the determination of strength and fracture toughness under contact loading. Test devices are described and solutions for the stress, the stress intensity factor, and the T-stress term are reported. Experimental results are compiled for the contact strength. For most investigated materials, measured contact strengths showed strongly reduced Weibull exponents compared with those from 4-point bending tests. This important effect is attributed to the strong stress gradients near the contact zone.*

## 1 Introduction

Conventional strength tests of brittle materials mostly describe the failure behaviour under simple stress states. These tests comprise uniaxial stresses with relatively small stress gradients. In most cases four-point bend tests with a linear stress distribution are performed. Predictions of the strength under more complicated stress states are possible - in principle - on the basis of the Weibull theory, including a multiaxial failure criterion (Batdorf and Heinisch, 1978; Evans, 1978; Matsuo, 1981). This approach is applicable at least in cases where the stress variations are small and sufficiently constant stresses can be assumed over the size of natural flaws from which the failure is initiated. The scatter of the strength is described by a two-parameter Weibull distribution, where the Weibull parameter m (see. eq.(21)) is independent of the stress distribution in the component. Under contact loading two damage modes are possible: the initiation of cracks in the compressive region under the indenter and extension of existing flaws under the tensile stresses near the indentation. Failure occurs usually by the unstable extension of these flaws. Due to the severe stress gradients the assumptions of the multiaxial Weibull theory no longer is valid.

In this paper a test method is described which allows the measurement of the contact strength. In addition, this device can be used to measure fracture toughness. It will be shown that the Weibull parameter *m* differs from that of bending tests and an explanation for this difference will be given.

## 2 Contact Strength Test

Fett et al. (2001a) developed a test for the direct determination of strength under contact loading. The test device is illustrated in Fig. 1. Two cylinders of 8 mm diameter made of hardened steel are pressed onto the rectangular specimen with a force *P*. The rollers are about 0.1 mm smaller than the guide groove in the supporting structure in order to avoid any clamping during load application (cylinders become oval under load).

For contact between the cylinders and the plane bar, the pressure distribution acting on the region $-s \le x \le s$ is

$$p(x) = p_0\sqrt{1-(x/s)^2}\ , \quad p_0 = \frac{2P}{s\pi t} \tag{1}$$

with the maximum pressure $p_0$ related to the total force *P* (Fig. 1). Under this load, the failure-relevant stress components can be computed from the Green's function given by Filon (1903), resulting in (Fett et al., 2001a)

$$\sigma_x = -2p_0\int_0^\infty \frac{1}{u}\frac{\sinh u - u\cosh u}{\sinh 2u + 2u}\cos\frac{ux}{H}\ J_1(u\,s/H)\cosh\frac{uy}{H}\mathrm{d}u$$

$$-2p_0\int_0^\infty \frac{y}{H}\frac{\sinh u}{\sinh 2u + 2u}\cos\frac{ux}{H}\ J_1(u\,s/H)\ \sinh\frac{uy}{H}\mathrm{d}u \tag{2}$$

$$\sigma_y = -2p_0\int_0^\infty \frac{1}{u}\,\frac{\sinh u + u\cosh u}{\sinh 2u + 2u}\cos\frac{ux}{H}\,J_1(u\,s/H)\cosh\frac{uy}{H}\mathrm{d}u$$

$$+\,2p_0\int_0^\infty \frac{y}{H}\,\frac{\sinh u}{\sinh 2u + 2u}\cos\frac{ux}{H}\;J_1(u\,s/H)\,\sinh\frac{uy}{H}\mathrm{d}u \qquad (3)$$

$$\tau_{xy} = 2p_0\int_0^\infty \frac{1}{u}\,\frac{u\cosh u}{\sinh 2u + 2u}\,\sin\frac{ux}{H}\;J_1(u\,s/H)\,\sinh\frac{uy}{H}\mathrm{d}u$$

$$-\,2p_0\int_0^\infty \frac{y}{H}\,\frac{\sinh u}{\sinh 2u + 2u}\sin\frac{ux}{H}\,J_1(u\,s/H)\;\cosh\frac{uy}{H}\mathrm{d}u \qquad (4)$$

with the Bessel function of first order, $J_1$. The maximum tensile stress of the bar is reached on the upper and lower surfaces, $y = \pm H$, directly near the rollers ($x \approx 0$). At these locations,

$$\sigma_{\max} = 0.490\sigma^*, \quad \sigma^* = \frac{P}{Ht} \qquad (5)$$

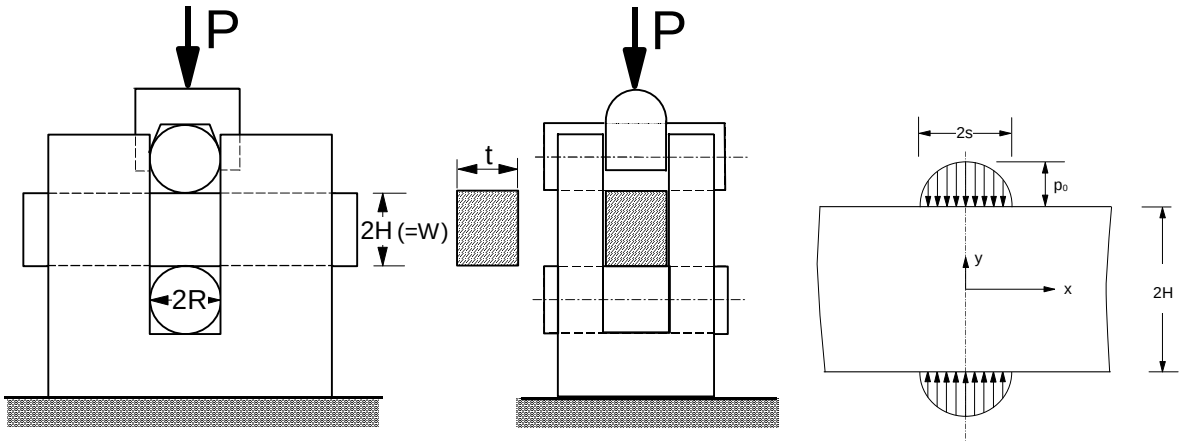


Figure 1. A two-roller test device for contact strength tests and Hertzian pressure distribution.

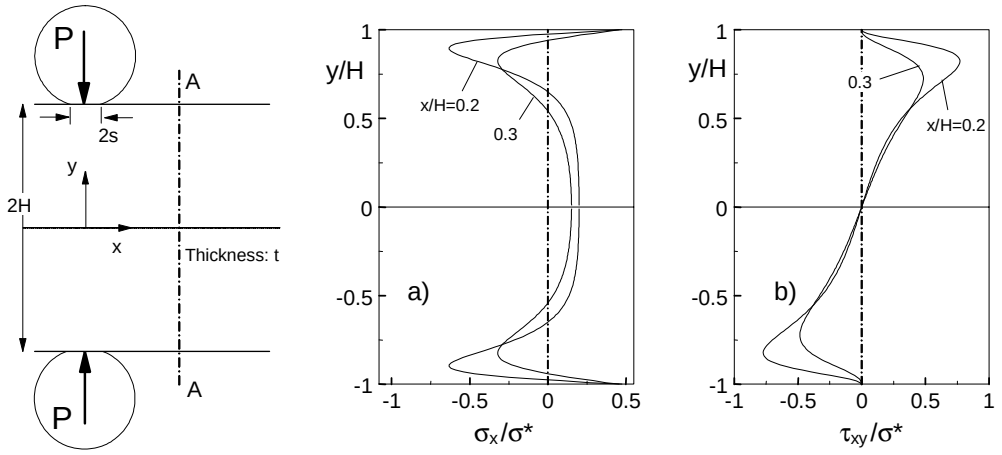


Figure 2. a) Geometric data of the two-roller test device b) stress normal to cross-section AA, c) shear stress in cross-section AA.

The stress state in a bar under contact loading by cylinders is demonstrated here for the case of $s/H = 0.1$. The stress components $\sigma_x$ and $\tau_{xy}$ are plotted in Fig. 2 versus the cross-section of the bar under contact loading. The stress component $\sigma_x$ is positive only in a very thin surface layer and then changes to compression. The shear

stress $\tau_{xy}$ is zero on the free surface and increases very strongly with increasing depth. The smaller the distance from the contact area is, the steeper are the stress gradients. The influence of the finite load contact area on the stress state is plotted in Fig. 3a along the free surface, i.e. for $y = H$. The maximum stress values (identical with the maximum tensile stresses in the whole specimen) occur near $x/H \approx s/H+0.025$. These maximum stresses (Fig. 3b) are influenced only slightly by the width of the contact zone. In realistic cases, the deviations from the maximum stress obtained as $s/H \rightarrow 0$ are less than 3%.

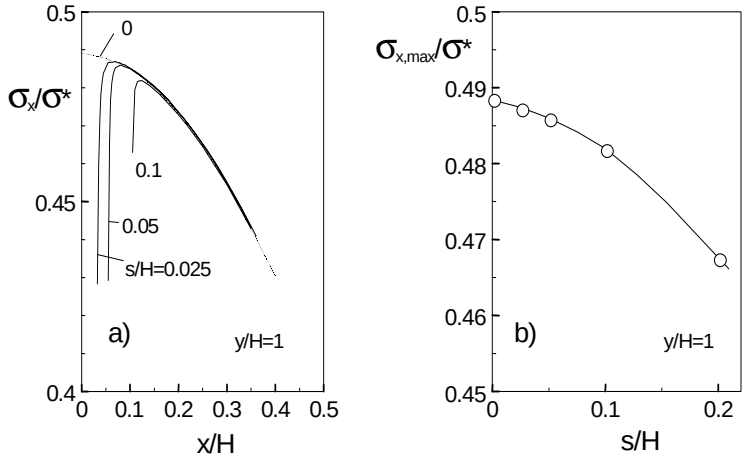


Figure 3. Influence of a finite pressurized zone: a) stresses $\sigma_x$ along the surface ($y = H$), b) maximum tensile stress on the surface.

## 3 Fracture Toughness Test

A modification of the contact strength test device (Fig. 4) is an appropriate tool to determine fracture toughness and crack resistance curves of ceramic materials (Fett et al., 2001a, Fett et al., 2001c). A pre-notched bar is loaded via four rollers in order to create a sharp crack. The load $P_{appl} = 2P$ is applied by a half-sphere to the upper rollers.

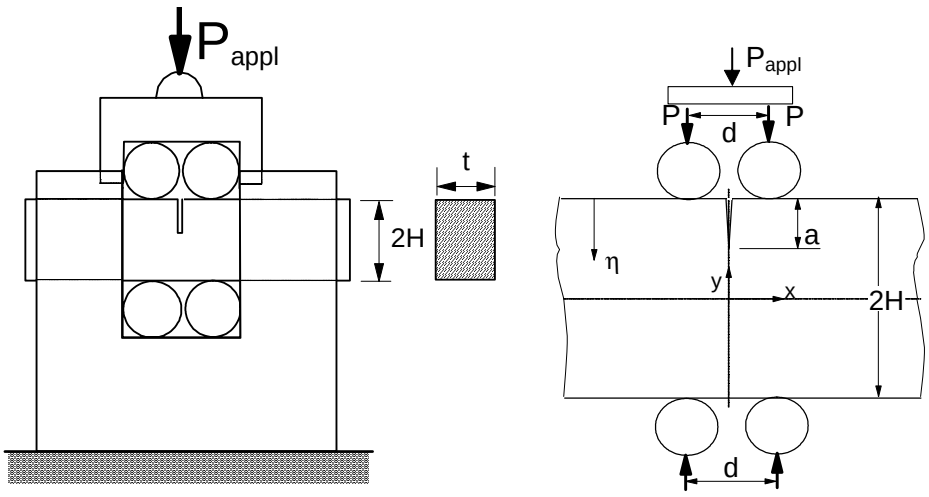


Figure 4. Four roller test device for fracture toughness determination

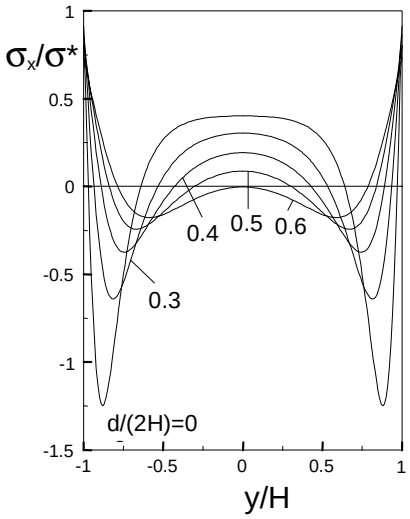


Figure 5. Axial stresses $\sigma_x$ along the symmetry line $x = 0$ for two pairs of concentrated opposite forces.

The stresses in the uncracked bar normal to the crack plane are shown in Fig. 5. Application of the weight function technique (for details see e.g. Fett and Munz 1997) yields the mode-I stress intensity factors $K_I$. The stress intensity factor is proportional to the applied load and depends on the ratios $a/H$, $d/H$ and a characteristic size parameter. Usually, this size parameter is the crack length $a$. Then

$$K_I = \sigma^* \sqrt{a} Y^*(a/H, d/H) \tag{6}$$

We use here the notation

$$K_I = \sigma^* \sqrt{H} Y(a/H, d/H) \tag{7}$$

with $Y = Y^* \sqrt{a/H}$ .

$Y$ is shown in Fig. 6 as a function of $\alpha = a/(2H)$ with $d/(2H)$ as a parameter. It is of high importance that for $d/(2H)=1$ the stress intensity factor firstly increases with crack length $a$, but then decreases monotonously. This causes completely stable crack propagation under increasing load. For the special case $d/(2H) = 1$, the geometric function $Y$ is fitted for $\alpha \le 0.6$ by

$$Y = 0.905\alpha^{1/2} - 3.358\alpha^{3/2} + 3.857\alpha^{5/2} + 1.4425\alpha^{7/2} - 3.873\alpha^{9/2} \tag{8}$$

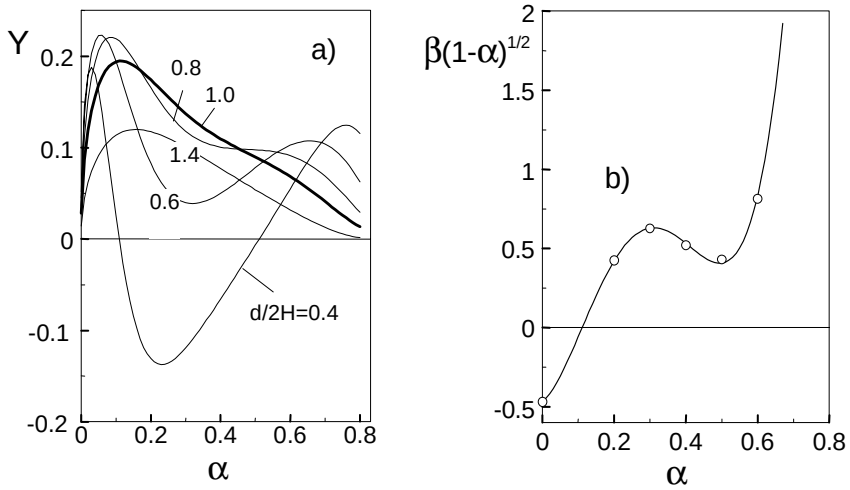


Figure 6. a) Geometry function $Y$ according to eq.(7) and b) biaxiality ratio $\beta$ for $d/(2H) = 1$.

In special applications, it may be important to know the stress field over a longer distance from the crack tip. This can be done by including higher-order stress terms. Taking into consideration the singular stress term and the first regular term, the near-tip stress field of a cracked body can be described by

$$\sigma_{ij} = \frac{K_I}{\sqrt{2\pi r}} f_{ij}(\varphi) + T\delta_{i1}\delta_{1j} \tag{9}$$

where $f_{ij}$ are the well-known angular functions for the singular stress contribution. The constant stress term is called the "T-stress". In Fig. 6b the biaxiality ratio $\beta$ is plotted, which is given by the ratio of the T-stress and stress intensity factor according to

$$\beta = \frac{T\sqrt{\pi a}}{K_I} \tag{10}$$

The curve given in Fig. 6b can be described (Fett et al., 2001b) by

$$\beta = \frac{-0.469 + 1.8589\alpha + 34.527\alpha^2 - 133.477\alpha^3 + 127.994\alpha^4}{\sqrt{1-\alpha}} \tag{11}$$

## 4 Experimental Results

### 4.1 Contact Strength

The authors measured the contact strength for several materials and in addition the bending strength applying four-point bend tests (Fett and Munz, 2002a; Fett et al., 2003). The results are described by the Weibull distribution. The probability that failure occurs below the stress $\sigma_c^*$ is:

$$F = 1 - \exp\left[-\left(\frac{\sigma_c^*}{\sigma_0}\right)^m\right] \tag{12}$$

The Weibull-parameters for the bending and the contact tests are called $\sigma_{0,\mathrm{bend}}$, $m_{\mathrm{bend}}$, and $\sigma_{0,\mathrm{cont}}$, $m_{\mathrm{cont}}$. In Fig. 7, the Weibull parameters are plotted. In this diagram, the rectangles represent 90% confidence intervals. The commercial alumina investigated were: V38, CeramTec, Plochingen (an alumina containing about 4 wt% glass phase), Frialit F99.7 ($d_m \approx 9\mu m$), and Frialit F99.9 ($d_m \approx 2.3\mu m$) both from Friatec, Friedrichsfeld. Frialit F99.7 was tested in two different surface states, denoted as materials F99.7(I) and F99.7(II). The other materials were a fine-grained AlN (CeramTec, Marktredwitz) and a low-strength HPSN (NH209, Annawerk, Rödental). The experiments on these ceramics yielded (Fett and Munz, 2002a; Fett et al., 2003)

- a linear relation between the Weibull parameters $\sigma_0$ for bending strength and contact strength with roughly

  $$\sigma_{0,\mathrm{bend}} \approx \sigma_{0,cont}$$

  as shown in Fig. 7a, where the 90% confidence intervals for the two tests are plotted
- lower Weibull exponents in the roller tests compared to the 4-point bending tests as shown in Figs. 7b and 7c by the 90% confidence intervals for the second Weibull parameter *m*. The only exception was found for the fine-grained $Al_2O_3$ (Frialit F 99.9). This material showed identical Weibull exponents in bending and contact loading.

From microscopic observation of fracture surfaces, it can be concluded that failure starts from surface flaws. In a recent paper, it could be shown that for cracks extending directly at the end of the Hertzian contact zone, the effective stress intensity factor depends linearly on the crack size. This behaviour results in reduced Weibull exponents for the strength (Fett and Munz, 2002a; Fett et al., 2003). In the present investigation, a more detailed analysis will be given.

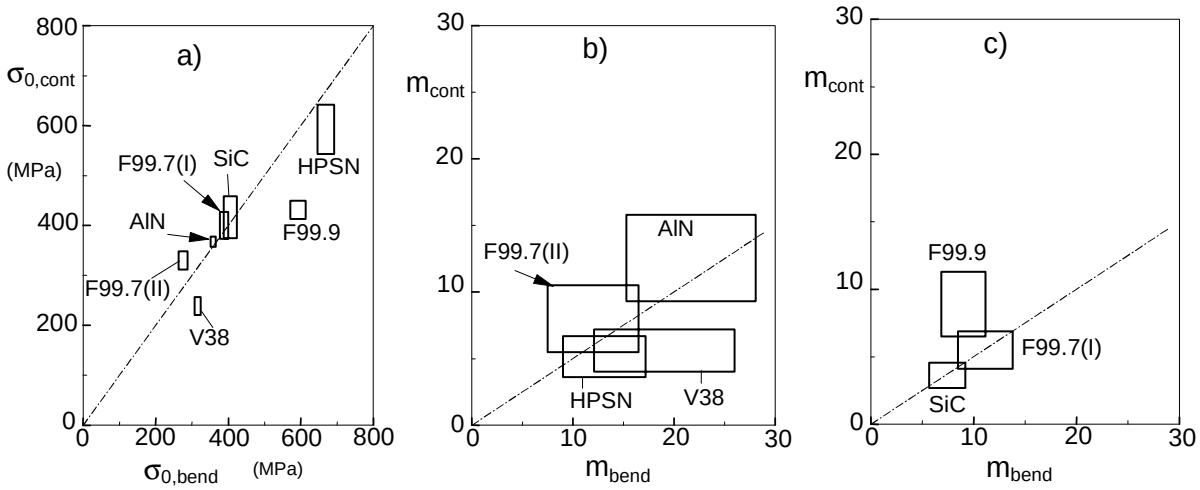


Figure 7. Interrelation between Weibull parameters of contact strength and 4-point bending strength tests; a) characteristic strength $\sigma_0$, b) and c) Weibull exponent *m* (widths and heights of rectangles given by the 90% confidence intervals).

### 4.2 Interpretation of Differences in Weibull Exponents of Contact Strength

The Weibull theory is a weakest link theory assuming that there exists a statistical distribution of flaws of different severity. In a fracture mechanics approach the flaws are described as cracks of different length *a*. The fracture criterion is under mode I loading (stress perpendicular to the crack plane) is

$$\sigma_c = \frac{K_{Ic}}{\sqrt{a} Y^*} \tag{13}$$

where $K_{Ic}$ is the fracture toughness. For the small natural flaws and moderate stress gradients $Y^*$ is independent of the flaws size *a*.

This assumption is approximately fulfilled for bending tests, but violated in a contact strength test near the loading cylinders. In order to include the strong stress gradients in the failure analysis the natural flaws are described as surface cracks perpendicular to the surface. From the stresses present in the uncracked body, the stress intensity factors $K_I$ and $K_{II}$ can be computed according to

$$K_I = \int_0^a h_I(\eta, a)\, \sigma_x(\eta)\, d\eta \tag{14}$$

$$K_{II} = \int_0^a h_{II}(\eta, a)\, \tau_{xy}(\eta)\, d\eta \tag{15}$$

with the weight functions $h_I$ for mode-I and $h_{II}$ for mode-II loading and the distance $\eta = H - y$ from the surface. The results obtained with the weight function solutions given by Fett and Munz (1997) are plotted in Figs. 8a and 8b, in a non-dimensional way (see eq.(6). From this representation, it is obvious that the mode-I stress intensity factors are positive close to the surface due to the tensile stresses near the free surface and then become negative at larger depths. In this case, at least partial crack closure must occur. The remaining stress intensity factor $K_{II}$ is reduced by crack surface friction.

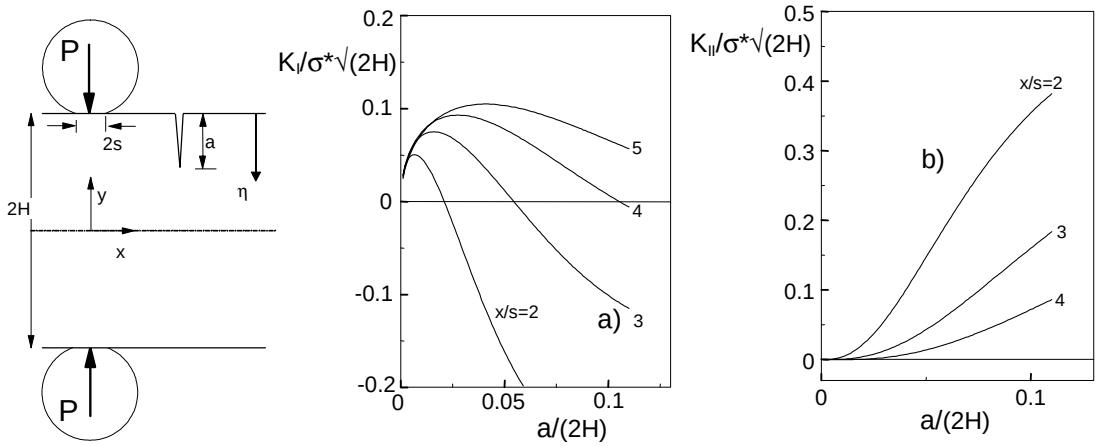


Figure 8. Stress intensity factors for edge cracks, a) mode-I and b) mode-II stress intensity factor ($s/H = 0.1$).

The effective stress intensity factor $K_{\text{eff}}$, combining $K_{\text{I}}$ and $K_{\text{II}}$, was computed by the empirical Richard formula (Richard, 1985). It provides the effective stress intensity factor (Fett and Munz, 2002b)

$$K_{eff} = \begin{cases} \frac{1}{2}K_I + \sqrt{\frac{1}{4}K_I^2 + \frac{3}{2}K_{II}^2} & \text{for} \quad K_I > 0 \\ \sqrt{\frac{3}{2}}(K_{II} + \mu K_I) & \text{for} \quad K_I < 0 \end{cases} \tag{16}$$

μ is the friction coefficient of the crack surfaces which has to be introduced for compressive normal stress at the crack. A value of 0.5 was chosen. The resulting effective stress intensity factors are shown in Fig. 9a as a function of crack depth $a$ and distance $x$ from the centre of the Hertzian contact zone. Figure 9b shows that large cracks with $a/(2H) > a^*/(2H)$ (where $a^*/(2H) \cong 0.01$) will predominantly fail near $x/s = 1$, whereas smaller cracks fail at a larger distance from the Hertzian contact zone. For the cracks near $x/s = 1$, the slope in the log-log plot is ≈1 for both criteria. In case of a larger distance, the slope is ≈1/2, i.e.

$$K_{eff,\max} \propto \begin{cases} a & \text{for} \quad a/(2H) > a^*/(2H) \\ \sqrt{a} & \text{for} \quad a/(2H) \le a^*/(2H) \end{cases} \tag{17}$$

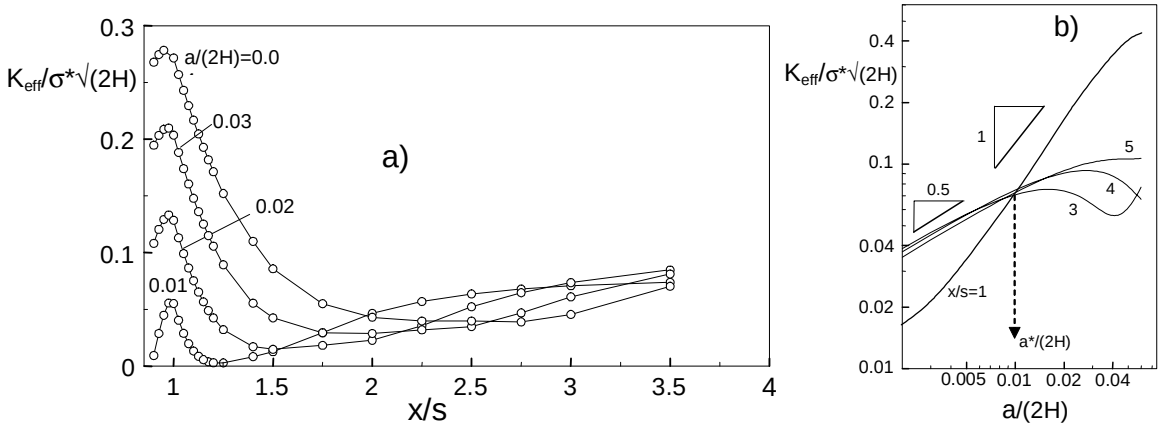


Figure 9. Normalized effective stress intensity factor $K_{\text{eff}}$, a) for variably deep edge cracks as a function of the distance $x$ from the contact centre, b) as a function of $a/(2H)$ for different $x/s$

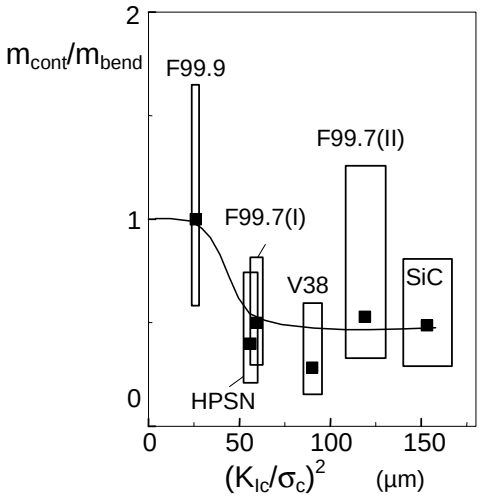


Figure 10. Ratio of Weibull exponents for contact and bending strength versus the initial crack size $a \propto (K_{Ic}/\sigma_c)^2$.

The different relation between $K_{eff}$ and the crack length leads to different Weibull parameters $m$. It is assumed that the asymptotic behaviour of the flaw size distribution can be described by a power law

$$f(a) \propto \frac{1}{a^r} \ , \tag{18}$$

From this relation the related strength distribution $F(\sigma_c)$ follows (for details see Munz and Fett, 1999)

$$F(\sigma_c) = 1 - \exp\left[ - zS \left( \frac{a_0}{a} \right)^{r-1} \right] \tag{19}$$

where $z$ is the number of cracks per surface unit and $S$ the surface of the component. Insertion of the relation between crack size $a$ and strength $\sigma_c$ in the form of

$$a \propto \sigma_c^{-p} \tag{20}$$

in (19) yields

$$F(\sigma_c) = 1 - \exp\left[ - \left( \frac{\sigma_c}{\sigma_0} \right)^{m} \right] \tag{21}$$

with the characteristic strength $\sigma_0$ and

$$m = p(r-1) \tag{22}$$

As a consequence of eq.(17), we obtain the usual value of $p = 2$ in the absence of strong stress gradients as in the bend tests

$$m_{bend} = 2(r-1) \tag{23a}$$

For the contact loading with $p$ =1 there is

$$m_{cont} = r - 1 \tag{23b}$$

i.e. the ratio $m_{bend} / m_{cont} = 2$ in agreement with the experimental results.

In Fig.7c an exception of the above can be seen for the material F99, for which the same Weibull parameter $m$ for both test methods was observed. An explanation can be given considering Fig.10 where the ratio $m_{cont}/m_{bend}$ is plotted versus $(K_{Ic}/\sigma_c)^2$. The ratio $(K_{Ic}/\sigma_c)^2$ is proportional to the size of the crack from which the fracture is initiated. Obviously for short cracks the Weibull exponents in both tests are identical, whereas for longer cracks lower exponents for the contact strengths are visible.

In the case of a large crack size (i.e. for large $(K_{Ic}/\sigma_c)^2$), it holds $a > a^*$ and from (17) $K \propto a$. For a small crack size with $a < a^*$ we have to conclude from (17) that $K \propto \sqrt{a}$. This difference leads to respective $m$-values differenting by a factor of 2.

### 4.3 Determination of the Fracture Toughness and Crack Growth Resistance

As pointed out in section 3 the four-roller test device can be applied to measure the fracture toughness. In most ceramics the crack growth resistance is not characterized by a unique value $K_{Ic}$, there exists rather an increase in the stress intensity factor with increasing crack extension (see e.g. Munz and Fett, 1999).

A result obtained for a commercial soft piezoelectric ceramic (PZT) is presented here as an example. V-notches within a range of depths of $a$ = 0.5-0.55 mm were cut into the unpoled and poled specimens of 3×4×45 mm$^3$ by the razor blade procedure (Nishida et al., 1996). The poling direction was parallel to the crack tip line with electrodes on the 4×45 mm$^2$ surfaces. Then, the specimens were loaded in the 4-roller testing device with $d/H = 2$ up to different forces. After unloading, the cracks generated were marked with a penetration dye and the length could be measured easily under the optical microscope following fracturing, thus providing the final crack depth $a$ (Fig. 11). From the load $P$ and the related crack length $a$, the stress intensity factor $K_R$ was computed according to eq.(7) with the geometric function $Y$ given by eq.(8). The results are plotted in Fig. 11.

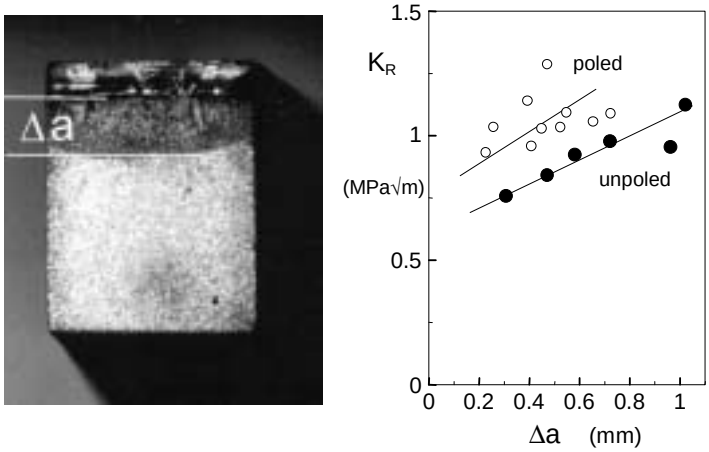


Figure 11. Crack resistance $K_R$ for unpoled and poled (poling direction parallel to the crack tip line) PZT as a function of crack extension.

**Conclusions**

Rectangular bars loaded by opposite concentrated forces via rollers are appropriate test specimens for the determination of the contact strength, the fracture toughness $K_{Ic}$, and the crack resistance curve (R-curve). In the paper the stress solutions for the cylinder contact tests are reported. For the fracture mechanics test, the stress intensity factor and T-stress solutions are given. The main results were:

- From contact strength tests on several ceramics it was found that the Weibull parameter, $m$, for the contact strength tests is about half that for bending tests. This could be explained by the strong stress gradients in the contact strength test.
- Due to the continuously decreasing stress intensity factor with increasing crack depth, unstable crack propagation is completely prevented in the cylinder contact tests. This advantage allows simple determination of crack growth resistance curves.

*Acknowledgement*: The authors would like to thank the Deutsche Forschungsgemeinschaft DFG for financing part of this work within the SFB 483.

**References**


Batdorf, S.B., Heinisch, H.L.: Weakest link theory reformulated for arbitrary fracture criterion, *J. Am. Ceram. Soc*. **61**(1978), 355-358.

Evans, A.G.: A general approach for the statistical analysis of multiaxial fracture, *J. Am. Ceram. Soc*. **61**, (1978), 302-308.

Fett, T., Munz, D.: *Stress Intensity Factors and Weight Functions*, Computational Mechanics Publications, 1997, Southampton, UK

Fett, T., Munz, D.: Influence of stress gradients on failure in contact strength tests with cylinder loading, *Engng. Fract. Mech.* **69**, (2002a), 1353-1361.

Fett, T., Munz, D.: Kinked cracks and Richard fracture criterion, *Int. J. Fract*. **115**, (2002b), L69-L73.

Fett, T., Munz, D., Thun, G.: Test devices for strength measurements of bars under contact loading, *Journal of Testing and Evaluation* **29**, (2001a), 1-10.

Fett, T., Munz, D., Thun, G.: A toughness test device with opposite roller loading, *Engineering Fracture Mechanics* **68**, (2001b), 29-38.

Fett, T., Munz, D., Thun, G., Hoffmann, M., Glazounov: A., On the interpretation of different R-curves for soft PZT, *Engng. Fract. Mech*. **68**, (2001c), 1207-1218.

Fett, T., Ernst, E., Munz, D., Badenheim, D., Oberacker, R.: Weibull analysis of ceramics under high stress gradients, *J. Europ. Ceram. Soc*. **23**, (2003), 2031-2037.

Filon, L.N.G.: On an approximate solution for the bending of a beam of rectangular cross-section under any system of load, with special reference to points of concentrated or discontinuous loading, *Phil. Trans*., *A*, **201**, (1903), 63-155.

Munz, D., Fett, T.: *CERAMICS, Failure, Material Selection*, Design, Springer-Verlag, März 1999.

Matsuo, Y.: A probabilistic analysis of fracture loci under bi-axial stress state, *Bull. JSME* **24**, (1981), 290-294.

Nishida, T., Pezzotti, G., Mangialardi, T., Paolini, A.E.: Fracture mechanics evaluation of ceramics by stable crack propagation in bend bar specimens, *Fracture Mechanics of Ceramics* **11**, (1996), 107-114.

Richard, H.A., Prediction of fracture of cracks subjected to combined tensile and shear loads (in German), *VDI Research Report 631/85* (1985), Düsseldorf, Germany.


---


Address: Dr. Theo Fett, Prof. Dr. Dietrich Munz, Institut für Materialforschung II, Forschungszentrum Karlsruhe, Postfach 3640, 76021 Karlsruhe, Germany

email: theo.fett@imf.fzk.de , dietrich.munz@imf.fzk.de